The use of STM to study metal film epitaxy

by D. D. Chambliss
R. J. Wilson
S. Chiang

In this paper we review work we have done at the IBM Almaden Research Center using the scanning tunneling microscope to understand the epitaxial growth of metal films. In particular, we explore the important role of deposit–substrate interactions in controlling growth and film structure, both by strain of the substrate and by place-exchange intermixing. These are illustrated first by the growth traits of Au, Ag, Ni, and Fe on Au(111) and their relationship to the herringbone reconstruction. Au on Ag(110) is presented as a clear example of spontaneous penetration of the substrate by deposited material at room temperature. Fe on Cu(100) is a more subtle example of the effect of place-exchange and of ways to observe it. The martensitic transformation of thicker Fe films on Cu(100) demonstrates the importance of bulklike structural changes in metastable epitaxial films.

Introduction

Epitaxy is the growth of a crystalline material on a crystalline substrate, so that the atomic arrangement of the growth is inherited from the substrate. With epitaxially grown thin films, one can investigate or exploit intrinsic properties of the material, including properties that are specific to particular crystallographic orientations, rather than of grain boundaries that can dominate the behavior of polycrystalline materials. A typical method for growing epitaxial thin films is molecular beam epitaxy (MBE), in which the substrate is exposed to a controlled flux of specific atomic or molecular constituents, usually supplied from devices in which the source material is heated to the point of evaporation or sublimation. This is done under conditions of ultrahigh vacuum (UHV) to protect the substrate and the deposit from contamination. Other means of delivering a film material to the surface can achieve some degree of epitaxial arrangement of the deposit, including magnetron sputtering, ion beam sputtering, chemical-vapor deposition, and electrochemical deposition. These different techniques are complicated by the presence of other atoms and molecules near the surface, but in all cases the mobility of deposited atoms, and their reactions with one another and with the substrate, play an important role in determining the structure of the film. The work described in this paper studies these phenomena in a relatively pure form, by examining very thin films deposited by evaporation/sublimation in UHV, an environment that resembles MBE growth. Since these studies have been of metal films, we observe bonding behavior and defect structures more representative of nondirectional metallic bonding than of directional covalent bonds in semiconductors.

0018-8646/95/$3.00 © 1995 IBM

The key concern in epitaxial growth is how the final arrangement of deposited atoms is determined by the substrate and deposit materials, and by conditions such as deposition rate and substrate temperature during growth. How are the structure and orientation of the film crystal (or crystallites) related to those of the substrate? What defects are introduced, both by the mismatch between substrate and deposit materials and by accidents of the growth process? What unusual structures, perhaps with desirable properties, arise for these same reasons? And, most fundamental, what is the film's "growth mode," i.e., does the deposit form a film of uniform thickness that entirely covers the substrate surface ("layer-by-layer growth"), or is there instead the growth of three-dimensional islands or other film roughness?

The scanning tunneling microscope (STM) is a superb tool for investigating the quality of epitaxial film growth because many of the essential questions about a film deal with what the STM measures easily: topography of the sample surface. Atomic steps and other height variations on a scale <1 Å are measured routinely. The step configuration shows whether islands have grown in only one atomic layer at a time or have grown atop one another to form three-dimensional growth. Thus, the processes that lead to film roughness can be examined at an early stage so that their origins can be understood. An added bonus is that the vacuum environment required for clean film growth also promotes the best performance of the STM. Without it, surface contamination of the sample or probe tip introduces additional noise that makes observation of atomic-scale features much more difficult.

The advantages of the STM notwithstanding, many essential questions about epitaxy cannot be answered without results from complementary techniques. The STM is a poor tool for measuring an unknown crystal structure, for although it is sometimes possible to produce an "atomic resolution" image that shows the surface lattice, even for close-packed metal surfaces, it is generally not possible to determine spacings and angles of atomic bonds precisely—which can be done routinely with diffraction measurements. Identification of different chemical species can be difficult or impossible with the STM because it is not directly sensitive to the electronic core levels that clearly distinguish different elements in electron spectroscopies. The valence-band electronic states near the Fermi energy, which determine tunnel currents in the STM, are sensitive to atomic species but in a less straightforward way. Similarly, no direct measurement of subsurface structure is possible with the STM, since it measures only the electrons at the surface. It turns out that all of these limitations can to some extent be overcome, at least in some cases, because crystallography, composition, and subsurface structure all have manifestations in the tunnel currents that determine STM images. By comparing with results from low-energy electron diffraction (LEED), Auger electron spectroscopy (AES), ion scattering, and other analytical tools, one can understand these effects well enough to observe, for example, specific variations in composition across a sample surface. This is analogous to a geologist's ability to identify minerals in the field by color, cleavage habit, etc., after the relationship of these traits to chemical composition and crystal structure has been determined in the laboratory. For both the geologist and the surface scientist, it is best if possible to make the analysis more exact by applying these complementary techniques to the same samples.

The slowness and intrusiveness of a proximal probe is another serious problem, for it implies that the STM cannot observe epitaxy while it occurs but can only examine the final surface. The repeated examination of one surface region after incremental deposition steps [1] reduces but does not eliminate the difficulty. In some situations there is no substitute for a probe that can measure structure during growth, such as reflection high-energy electron diffraction (RHEED). STM has been used to improve the usefulness of such probes, by establishing accurately what the probes measure for specific well-characterized surface structures [2–4]. In this paper we have emphasized another approach, namely the study of model systems to establish the general phenomena that are most important in epitaxy. The STM has offered evidence of the processes of atomic motion, nucleation, and growth as expected in conventional theories of film growth; it has also made clear that unexpected processes often have an impact on the growth behavior.

For epitaxial film growth to work, the free energy of the desired film structure must be a local minimum that can be reached during deposition. It is rarely, if ever, a *global* minimum, which for miscible materials is usually an alloy or compound, and for immiscible materials often involves three-dimensional clusters that minimize the interface area. Thus, a substrate temperature must be found that is high enough to facilitate some structural equilibration within the film, but low enough to maintain the integrity of the film itself. This requires as a minimum that deposited atoms be highly mobile on atomically flat terraces, and that bulk interdiffusion be negligible. In the studies reviewed here, however, it has been found that many other atomic processes are important. Mobility of atoms along and across steps, relaxation of substrate stress structures, and atomic exchange between deposit and substrate play a considerable role in determining the step density during growth, the breadth of the interface, the roughness of the final surface, and the structural perfection of the film. These characteristics may not always be important in thick films, but they can be a major concern when layers only a few atomic planes thick are incorporated into devices. We

have also found that subtle effects are more likely to arise in the growth of metal films than they are in semiconductor epitaxy, where strongly directional covalent bonds restrict the possibilities of defect structures. Just as defects like dislocations and stacking faults are more common in bulk metal crystals, so the variety of mechanisms to relieve stress and lattice mismatch seems also to be greater.

The carefully prepared single-crystal substrates used most often in MBE consist mainly of atomically flat terraces separated by relatively few atomic steps [**Figure 1(a)**]. Atoms landing on these surfaces can generally move rapidly to preferred adsorption sites at steps. Thus, during deposition there is a dilute gas of these "adatoms" (adsorbed atoms) which is continually being depleted by absorption at steps and replenished by deposition. While most mobile atoms do not encounter other mobile atoms before sticking at steps, the encounters that do occur are important because they lead to island nucleation on otherwise featureless terraces. Qualitatively, a low adatom diffusivity D combined with a high deposition flux F is more likely to lead to island nucleation and a somewhat rougher film [**Figure 1(b)**], while a larger value of the ratio D/F may lead to step flow growth [**Figure 1(c)**]. Quantitative aspects of nucleation and growth have been studied extensively using theory and modeling [5]. It is assumed in most theoretical treatments that the substrate is unchanged by film growth and that single atoms move independently in the potential energy function defined by the substrate and by one another. These studies have been quite successful in some areas, and predictions have been borne out by later STM measurements. At the same time, STM and other experimental methods have shown that intimate interaction with the substrate and cooperative motion of several atoms are phenomena of more widespread importance than had been appreciated, and new theories are being developed to incorporate these important ingredients.

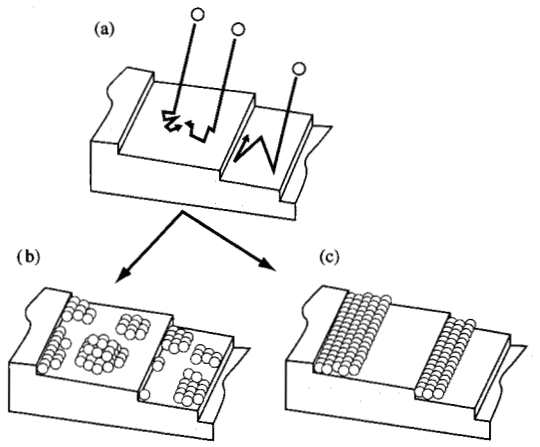

Figure 1

Atom deposition and aggregation during MBE: (a) Substrate surface consists of atomically flat terraces, separated by steps. Deposited atoms land and diffuse on terraces. They may encounter one another (as shown on upper terrace) or migrate to the step and adhere there. (b) Island growth results from higher deposition fluxes and more adatom–adatom encounters. (c) Aggregation at steps may dominate for lower flux.

Experimental techniques

We have conducted experiments by depositing controlled amounts of metal onto well-polished metal crystals in UHV, and examining the results with an STM soon after deposition. The vacuum apparatus we used [6] permitted the sample to be moved between positions for deposition and for STM measurement without exposure to significant contamination. It also offered facilities for LEED and AES measurements. The single-crystal metal substrates were mechanically cut and polished to the correct orientation (within 0.5°) before they were introduced into the vacuum system. They were cleaned by sputtering (i.e., bombardment with 500–1000-eV Ar ions), to remove several atomic layers and therewith any surface contamination, and were heated to activate step mobility on the surface (typically 600°C), so that holes and peaks formed by sputtering could be smoothed out. Samples prepared this way still have many atomic steps, since the mechanical polishing plane is not perfectly aligned to the crystallographic plane, and since any roughness left by polishing or sputtering is very slow to anneal away for length scales comparable to 1 μm. The atomically flat terraces between steps are typically tens to hundreds of atoms wide. The steps may tend to bunch because of thermodynamic or kinetic factors, which then leaves many very narrow and a few very wide terraces. Most of the present work concentrates on the growth behavior on wide terraces, regarding steps as a local perturbation that becomes dominant in highly stepped regions of the surface.

Metal films were deposited using fairly simple evaporators. Sophisticated and expensive evaporators would be needed to ensure a constant, well-controlled rate and uniform deposition across a substrate, but for STM studies of submonolayer deposits, neither precise rate control nor uniformity was crucial. Thus Ag, Au, and Ni were evaporated from resistively heated alumina-coated tungsten-wire baskets. Fe was evaporated from a mass of Fe wire heated by electron bombardment from a nearby heated filament. An important parameter is the total dose of evaporant on the surface, which may be estimated by using AES or by appropriate monitoring of the evaporator. In many cases the most accurate measurement of this

coverage comes from the STM images themselves. The conventional unit of coverage is the "monolayer" (ML), defined as the amount of material needed to cover the surface with a single deposited layer. Deposition rates, typically between 0.1 and 10 monolayers per minute, were estimated from the total deposit and the elapsed time. For Fe and Au deposits greater than 1 ML, the deposition rate was monitored using an ionization gauge in the periphery of the evaporant beam [7]. The "pressure" reading on the gauge was calibrated using submonolayer deposits.

We used the STM in the conventional "topographic" mode, in which a nearly constant tunnel current is maintained in a feedback loop during scanning, so that the tip describes a trajectory of nearly constant distance from the surface atoms. Tunnel current was monitored (but usually not recorded) to ensure that the loop accurately tracked the surface. Certain inaccuracies of the STM were corrected. Thermal drift and piezoelectric creep in our instrument implied that the region scanned by sweeping x and y voltages was usually a skew parallelogram rather than a square. This skewing was estimated by comparing forward and reverse scans, and was then removed by a geometric transformation of the data. This is the reason for the nonrectangular shape of images in some figures. Quadratic backgrounds were also subtracted, to correct for piezoelectric element properties, and in some cases a line-by-line leveling algorithm was applied to remove the apparently random stepwise height fluctuations that result from motion of atoms on the probe tip near the tunnel junction. When images were analyzed quantitatively—as when measuring island areas to determine coverage—efforts were made to compensate for the broadening effect of the tip, generally by appropriate adjustment of thresholds. The data are generally presented as a "plan view" gray-scale image in which darker shades denote "lower" sample points (i.e., where there was less sample material and the tip extended outward to maintain constant current) and lighter shades are higher points (e.g., aggregates of deposited material). In some cases a numerically differentiated image is presented that resembles what would appear if a three-dimensional model were illuminated from the left. In some images, small height variations are magnified so that they will be visible when images are reproduced.

Growth of Au, Ni, Fe, and Ag on Au(111)

The growth of Au on Au(111) illustrates some of the subtleties of surface structure that can be learned with the STM and have significant effects on growth. A (111) lattice plane within the face-centered-cubic (fcc) Au crystal is a hexagonal array of atoms, all in equivalent positions. If the Au(111) surface kept this structure, the flat terraces between atomic steps would appear featureless, except that contamination or the atomic lattice might be visible. Instead, the surface *reconstructs*, shortening its nearest-neighbor distances to compensate for the smaller number of neighbors (9, instead of 12 in the bulk). The details of this reconstruction were revealed first using helium atom scattering [8] and were amplified upon using STM [9–11]. The distances between atoms in the plane are reduced so as to pack about 4% more atoms per unit area than in interior (111) planes. Thus, the top layer of pure Au, because it is at the surface, behaves almost like a different material, with a different natural lattice constant, from the "substrate." This is analogous to the *lattice mismatch* that is important when a film and its substrate are of different materials ("heteroepitaxy"). The surface–bulk mismatch here yields structures analogous to the misfit dislocations often produced during heteroepitaxy. These are seen in STM images as slight ridges about 0.16 Å high [light bands in **Figure 2(a)**]. The simple dislocations separate into two partial misfit dislocations, so each added row of atoms in the surface appears as a pair of parallel ridges about 20 Å apart. The region separating these parallel pairs is referred to as a "stacking fault" region because the surface atoms there are positioned relative to the next two layers as if the crystal structure were hexagonal close-packed (hcp) rather than fcc.

The long-range appearance of this reconstruction reveals how different regions of the surface can interact through the substrate to produce an ordered structure. We observe in STM images that the ridge pairs consist of straight segments, along specific crystallographic directions ($\{\bar{2}11\}$), except in junctions between straight sections. On a flat terrace of the annealed Au(111) surface, the straight segments alternate between two of the three possible directions, and the zigzagging ridges describe a "herringbone" pattern [Figure 2(a)].

This alternation can be explained using linear elasticity theory [12]. A surface region containing dislocations of this kind aligned in a single direction (a "uniaxial domain") accommodates misfit only in one direction. The unrelieved stress in the orthogonal direction induces a strain field in the crystal, whose elastic energy per unit surface area would grow without bound if the uniaxial region extended infinitely. When uniaxial domains of different orientations coexist side by side, the bulk strain fields tend to cancel, so it is energetically favorable for the globally averaged surface stress to be isotropic. Boundaries between uniaxial domains involve a variety of defect structures (discussed in greater detail below) with different energy costs; the trade-off between these costs and the corresponding gains in bulk strain energy determines the type of long-range structure that is formed, and the length scale. While for Au(111) and some other systems the result involves the herringbone in which two of the three uniaxial directions will alternate, in other cases the local ordering involves a mixture of all three directions [13, 14]. Since the

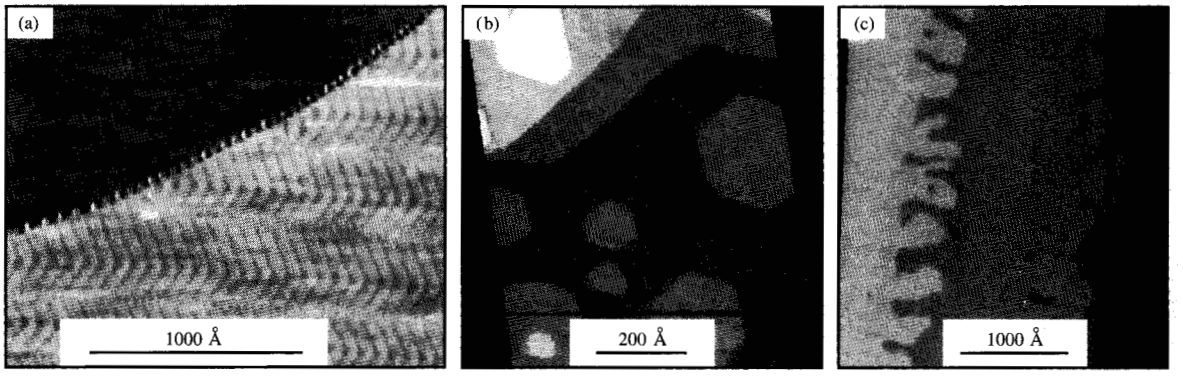

Figure 2

Epitaxy on reconstructed Au(111): (a) "Herringbone" reconstruction of Au(111). Two terrace levels are shown; black and white dots along step are an artificial result of image enhancement. (b) Au islands grown on Au(111) (coverage $\theta = 0.3$ ML). (c) Ag fingers growing from step edges on Au(111) ($\theta = 0.25$ ML).

herringbone pattern involves two uniaxial directions, not three, global symmetry requires the existence of regions with all three possible pairs. These are indeed found on the surface, typically in regions separated by steps. The herringbone pattern of Au(111) has a nearly constant half-period of 140 Å in our STM data. This period depends on annealing temperature and quench rate [11, 15]. A temperature dependence at equilibrium should arise because of the entropic contribution to the free energies of the surface defects. The mobility of the defects is low in a room-temperature STM, so the structure we measure is frozen in at some higher temperature.

It is not obvious *a priori* how deposited metal atoms and this surface reconstruction might interact, even in the simplest case of homoepitaxy [Au on Au(111)]. If a substrate is viewed as essentially unchanged by growth of islands from deposited material, one would expect that any structure seen in the overlayer would be an echo of the original herringbone pattern. One might find rectangular islands aligned to the local uniaxial strain, or a conformal layer in which the dislocation ridges are seen but are broadened because they are buried deeper. However, the STM results refute these expectations [**Figure 2(b)**] [16]. If the fine-scale topography of the surface is ignored, there appears to have been simple growth of 2D islands, the beginning of good layer-by-layer growth. The observation of relatively large islands indicates that the Au atoms were highly mobile after being deposited. Their clear hexagonal shape shows that close-packed step edges are energetically preferred, and that atoms are mobile enough to attain this low-energy shape. The complexity of this growth is found in the reconstruction. The islands and exposed substrate areas are all reconstructed, with the same local structure as before: straight low ridges in parallel pairs, with the same spacing. This makes energetic sense, since the deposited layer just makes a new Au surface on the substrate. The dislocations that make up the reconstruction have not simply moved up by one atomic layer, however, for the long-range herringbone order is lost. Instead, straight dislocation segments are strongly correlated in orientation to nearby island edges, in almost all cases running perpendicular to them. The new topography shows that island growth has removed the dislocations between the first and second substrate layers, and replaced them with dislocations between the first substrate layer and the first deposited layer.

The behavior of deposited Ag on Au(111) is markedly different [**Figure 2(c)**], although there are some similarities [17]. Again, the growth is nearly perfect layer by layer. Almost all of the deposited Ag, however, contributes to deposits at steps, and almost no islands are formed. Since rates comparable to that used for Au deposition were used, this suggests either that Ag atoms separately have greater mobility than Au atoms, or that more Ag atoms are required to form a stable island cluster. More surprising is the distinctive fingerlike shape of the deposits, which resembles the results of certain viscous flow experiments rather than the faceted Au islands. A tendency toward ramified growth can be explained in part by the mathematics of diffusion-limited aggregation (DLA) [18, 19], which in appropriate limits yields fractal deposits. An atom that walks randomly on the surface until reaching a step is most likely first to reach a step segment that protrudes onto the open terrace; when it attaches there,

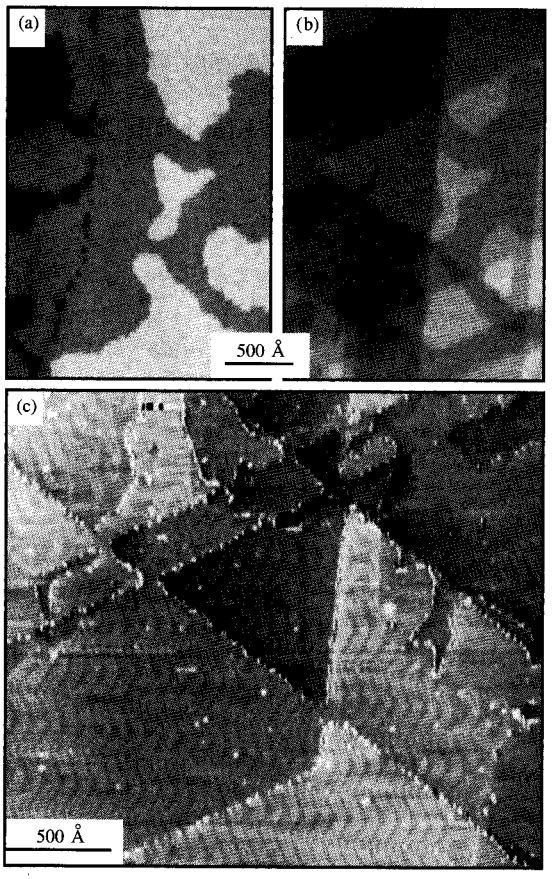

Figure 3

Ag films on Au(111), modified by "nanojackhammer": (a, b) Au(111) + 1.6 ML Ag, before (a) and after (b) a tip crash induced slip faults in the sample. (c) Au(111) + 0.1 ML Ag. Flat surfaces are broken by straight steps due to a tip crash. Black and white dots near steps are artifacts of image enhancement.

the protrusion grows longer. This tends to amplify statistical fluctuations in the step position. It might have been expected that a high mobility of the atom on a flat terrace would imply high mobility along the step or a high probability of leaving the step and reattaching elsewhere, which would suppress the amplification of roughness. Experimentally, however, one can find examples where islands exhibit the fractal shape expected if such smoothing effects are limited [20].

The fairly round contours of the Ag deposits do not resemble closely the highly ramified structures of DLA. One might imagine, however, that a DLA aggregate could gradually become more compact as atoms rearranged themselves to reduce the total energy. In such a coarsening process, the fine-grained step roughness would disappear quickly, and the typical radius of curvature of structures would grow over time. An experimental accident helped us rule out this explanation for the characteristic shape of Ag fingers. A fault in our control electronics caused sporadic crashes between tip and sample in the STM. It would try to plunge the tip nanometers below the crystal surface, then withdraw it. These "nanojackhammer" impacts obliterated the original topography of the contact region, but we could recover reasonable imaging conditions with the same tip over nearby areas. We found the impacts disrupted the neighboring regions, to a distance of several microns, by introducing numerous slip faults along close-packed planes of the bulk crystal. The faults show up in STM images as straight steps along crystallographic directions. Examples of this appear in **Figure 3**. Parts (a) and (b) show one region of a sample before and after such an event about one micron away. This sample has 1.6 ML of Ag on Au(111). Aside from the introduction of straight steps, there is almost no difference between the images: Polygonal regions have simply been raised or lowered. The sharp corners formed in this process show almost no sign of the atomic rearrangement one would expect if gradual coarsening were responsible for the shapes of Ag deposits. Since it seems that a sharp corner, once formed, will stay that way for a long time, it follows that the Ag fingers are rounded because they were formed that way. In images of submonolayer deposits [Figure 3(c)], we can see how the clean Au responds to the introduction of new steps by the nanojackhammer.

What must be included to account for the shape of Ag deposits is the interaction of aggregation with the Au(111) reconstruction. The Ag deposits for the most part appear quite flat, showing neither the ridges of reconstructed Au nor the broadened features one would expect to find if the Au reconstruction were buried intact. (In the open crystal structures of semiconductors, a defect might be buried with little or no topographic evidence at the surface, but this is unlikely with these metal atoms because they tend to pack closely. Indeed, in some places the erasure of the reconstruction discussed below is incomplete, and a few buried dislocations are seen with the STM as broadened ridges.) This means that a growing Ag cluster must somehow remove the dislocations. While STM images show only results and not cause and effect *per se*, the correlation between Ag cluster boundaries and straight segments of dislocations suggests that these segments behave as firm but not immovable barriers to growth. This correlation is seen in **Figure 4**, and shows up differently at the ends of fingerlike clusters (where growth is continuing) and at their sides. At the ends the Au reconstruction exhibits considerable disruption, in which the dislocation ridges show new connections not found in the herringbone pattern on clean Au terraces. This is apparent in the upper

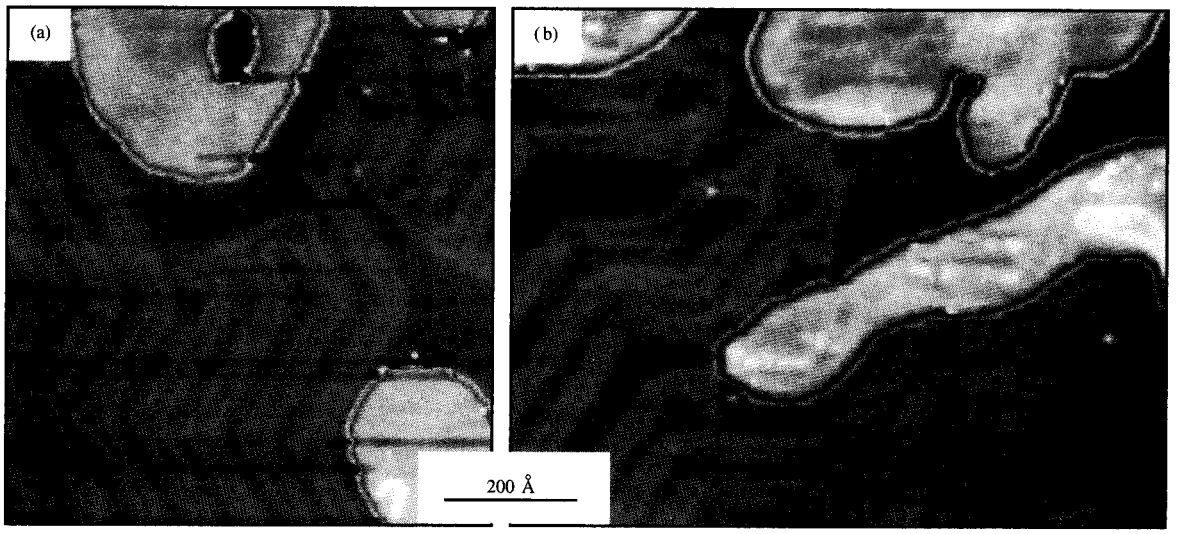

Figure 4

Correlation of Ag deposits to Au(111) reconstruction. Coverage: 0.16 ML Ag on Au(111). The black and white bands along steps are artifacts of the image enhancement used to make the reconstruction visible.

parts of Figures 4(a) and 4(b). This suggests that the reconstruction tends to "retreat and regroup" before the advancing Ag cluster edge. At the sides, though, the Ag step often exhibits the same zigzags as the reconstruction ridges of the neighboring uncovered Au surface. This is seen most clearly below the center of Figure 4(b) and also to some extent at the lower right of Figure 4(a). We note that these zigzags are just a continuation of the same herringbone pattern on the more distant parts of the Au terrace. This suggests that this part of the herringbone has not been changed by Ag growth. That is, here it seems that the growth follows the reconstruction, not vice versa. One possible description of the process is that the dislocation ridges present a barrier to Ag aggregation, which therefore occurs preferentially where the reconstruction has already been removed. Sometimes growth cannot proceed unless the barrier is broken through, and when the reconstruction is thus disrupted it leaves a new area where aggregation again occurs with relative ease. If the dynamics of removing the reconstruction play an integral role in determining the morphology, it is not surprising that that morphology is not well reproduced in models such as DLA that assume single atoms diffusing on a featureless substrate.

A remarkable lesson from both Au and Ag growth on Au(111) is that they invalidate the appealing view of the substrate as an inert and immutable base for growth. It is not surprising that growth would disrupt the reconstruction, since once the substrate surface is buried there is no longer a driving force to push it away from the bulk-stable configuration. But the dislocations accommodate a 4% increase in atom density, so removing them requires finding a new home for those atoms. For each unit-cell length of dislocation moved out of the surface layer, a Au atom must move out with it. Since this surface-atom extraction occurs during growth, one must expect it to influence significantly the adatom attachment–detachment probabilities that are used to account for island shapes and sizes.

Whereas Ag and Au are very similar in size and chemistry, they are very different from the magnetic materials Ni and Fe. The morphology of Ni or Fe deposited on Au(111) is likewise very different from that of Ag and Au. The Ni or Fe atoms form monolayer-high clusters in regular arrays [**Figure 5(a)**]. The island positions are determined by the herringbone structure of the reconstructed substrate. Several hypotheses arise as explanations of this structure, including the effect of the reconstruction on adatom diffusion, and the periodically varying surface strain in the reconstruction, which could affect stability of clusters. While these cannot be ruled out as minor influences, experiments make clear a simpler explanation [21]. Each island nucleates at a point defect of the surface lattice that must be present as a consequence of the reconstruction. The defect is a dislocation of the surface lattice, a point at which an "extra" row of atoms

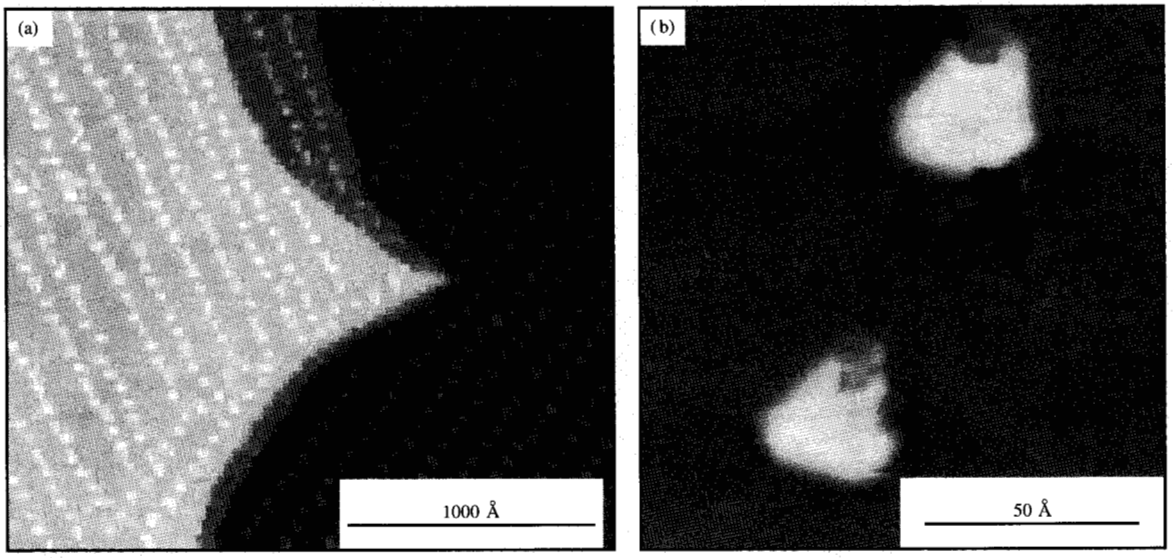

Figure 5

Nucleation of island arrays by Au(111) "herringbone" reconstruction: (a) Ni islands formed by submonolayer deposit. Each light dot is a Ni island one layer high containing 100–200 atoms. $\theta = 0.1$ ML. (b) Magnified view of Fe islands in array ($\theta = 0.03$ ML). Near upper island is a large dark patch that is interpreted as possible Fe incorporated into the Au surface. In both images, islands are 73 Å apart, and island rows are separated by about 140 Å.

begins or ends. This is the same surface structure as would result if an edge dislocation emerged from the bulk. No bulk dislocation is actually present, however; the surface dislocation is just the junction of two partial misfit dislocations (which produce the ridges in STM images) that have unequal Burgers vectors. At the defect site there must be surface atoms with bonding geometries highly distorted from the preferred hexagonal arrangement, and these atoms offer favorable sites for Ni or Fe atoms to stick and form islands.

We note that the formation of a spontaneous ordered structure like these island arrays is intriguing in the study of nanostructured materials. One hopes that such a starting point may permit the growth of a huge number of tiny magnets, for example, with a well-controlled spacing and size. An important lesson of these studies of epitaxy, and of this paper, however, is that each stage of growth presents many opportunities for the desired structure to be destroyed. It will be a considerable accomplishment when spontaneous ordering at the nanometer scale can be exploited to produce materials with novel properties.

Images of Fe deposited on Au(111) reveal the extra complication of deposited atoms mixing into the substrate. Near most islands are patches of the substrate surface that appear under some imaging conditions as if they were holes [**Figure 5(b)**]. Interpretation of such features is difficult, since the arrangement and identity of atoms on the tip is an unknown variable with considerable influence on the tunnel current. It is clear, however, that these patches cannot be an undisturbed Au lattice with a structure like the rest of the substrate. A large, bias-dependent apparent height difference is most often due to a difference in composition. In this case the patches are probably regions where deposited Fe atoms have replaced Au atoms, and the displaced Au atoms have presumably become incorporated into the islands. The driving force could be the higher surface energy of Fe than of Au, so that it is energetically advantageous to break Au–Au bonds in order to make more Fe–Fe or Fe–Au bonds. It is unlikely that this would occur by first creating a Au vacancy and later filling it with an Fe atom, since the activation energy for creating a vacancy is high. It could occur via a cooperative atomic "place exchange" in which the Fe atom moves in as the Au atom moves out, and a bare vacancy is never created. Such exchanges have been predicted and demonstrated on several fcc(100) surfaces [22, 23]. Although place exchange should be more difficult on a packed (111) surface, the distorted geometry near the surface dislocations is presumably a less tightly bound

structure for which atomic rearrangements are much easier.

Intermixed Stranski–Krastanov mode for Au on Ag(110)

A comparable exchange of deposited atoms with the substrate proves to be a dominant process in the initial growth of Au on Ag(110) [24]. Here the essential step in our understanding has been to reconcile STM data with ion-scattering experiments, which showed that many deposited Au atoms were found to be buried [25]. The original interpretation was that Au atoms aggregated into bilayer islands, so that half of the Au atoms were covered by other Au. The STM study showed clearly, however, that the two-atom-high steps and islands such a growth mode must create were not present. Indeed, in initial stages no islands were found; the main change seen was that Au deposition made the step shapes more stable. Au and Ag atoms could not be distinguished clearly in STM images, but the combination of STM and ion-scattering data showed that the Au atoms must interchange with Ag atoms to bury themselves below the surface. This model [**Figure 6(a)**] [24] has been shown to be quantitatively consistent with the ion-scattering data, and has been shown to be energetically favorable by first-principles calculations [26]. Recent molecular dynamics simulations have confirmed that the exchange processes needed to reach this model are possible at relatively low temperatures [27]. After the surface is covered with the mixed Au–Ag surface, Au deposition then leads to three-dimensional island growth. This transition to 3D growth is a variation of Stranski–Krastanov growth, and the STM study found clear examples of the early formation of 3D islands [**Figures 6(b)** and **6(c)**].

Low-coverage Fe on Cu(100): Intermixing

In retrospect it is not at all surprising that intermixing should occur for Au on Ag(110). The two elements are completely miscible, so alloy-like structures are not energetically costly, and the comparatively open atomic geometry of an fcc(110) surface makes place exchange possible with fairly small bond distortions. The next system we discuss, the growth of Fe on Cu(100), is considerably different. First, the fcc(100) surface is more closely packed than fcc(110). This does not preclude place exchange, which is known to occur on some fcc(100) surfaces. Indeed, we determined that place exchange is the dominant mechanism for the formation of the $c(2 \times 2)$ alloy of Au on Cu(100) [28]. A more important difference is that Fe and Cu do not form bulk alloys, so Fe atoms in Cu tend to form Fe clusters if their mobility is sufficient. Thus, it appears that thermodynamics should operate against intermixing, at least below the high temperatures at which some solubility of Fe in Cu is observed.

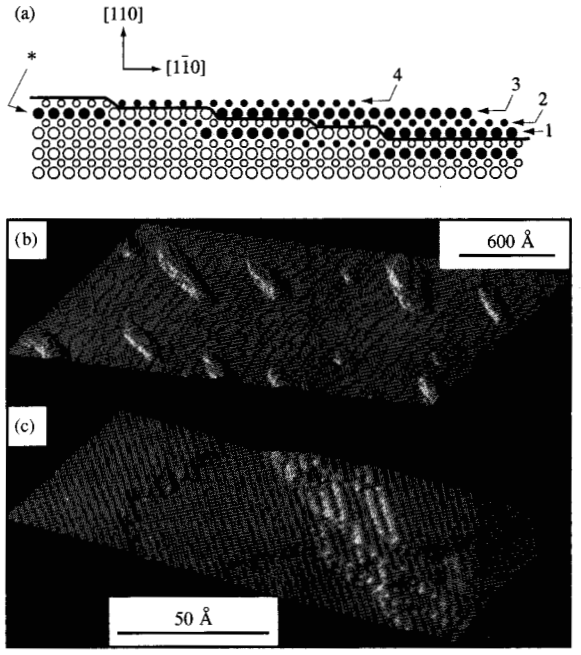

Figure 6

Intermixed Stranski–Krastanov Au growth on Ag(110): (a) Cross-section atomic model. Dark circles are Au atoms; open circles, Ag. The initially deposited Au penetrates below the Ag surface (*). Later growth is in fingers, one atop another (1, 2, 3, 4) to start growth of 3D islands. (b, c) STM images of 3D island growth at $\theta = 1.8$ ML. A 3D rendering is shown using equal scale factors for x, y, and z. Meandering lines in (b) from lower left to upper right are substrate steps. In (c) the individual atomic rows constituting an island are seen.

Nevertheless, intermixing at or near room temperature does occur, and exerts considerable influence on the growth characteristics. Prior studies of Fe growth on Cu(100) found evidence for intermixing at slightly elevated temperature, as well as for bilayer islands at room temperature [29, 30]. As was the case for Au on Ag(110), STM found a preponderance of one-atom-high steps in the initial stages, and too little growth at the second layer to support a bilayer-island model. While the previous studies had shown that many Fe atoms were below the surface, and that Cu atoms remained exposed at the surface, they did not identify what atoms covered the buried Fe atoms, or where they lay relative to the starting surface. Thus, a range of structural models were considered in order to find one that explained both the early burying of Fe atoms and the monolayer topography found with the STM.

The model supported by our STM results, and consistent with most or all other experimental data, is shown in **Figures 7(a)** and **7(b)**. An Fe atom landing on the

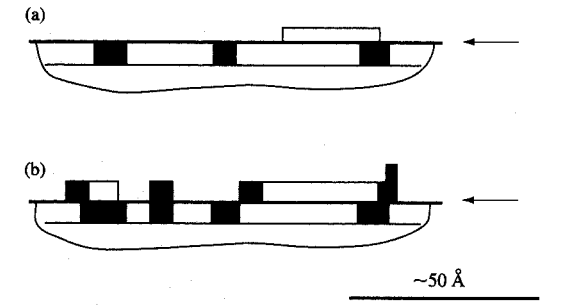

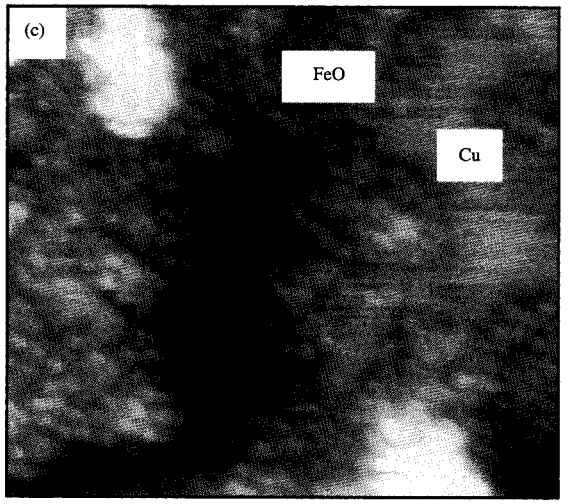

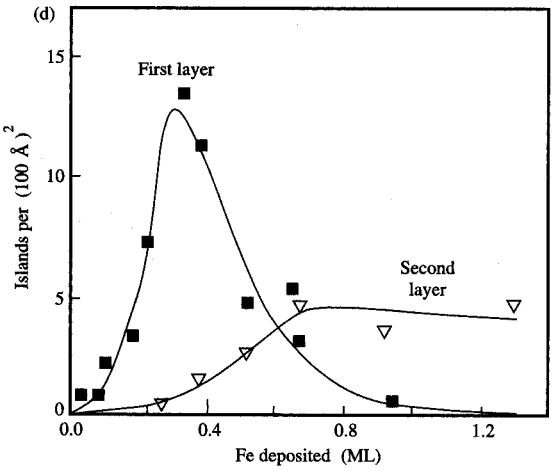

Figure 7

Structure of submonolayer Fe on Cu(100): (a) Cross-section model of surface structure after 0.1 ML of Fe is deposited. Dark regions are Fe clusters embedded in the surface. (b) Surface structure after 0.5-ML deposition. (c) STM image of oxidized 1-ML deposit. (d) Island nucleation as a function of Fe deposition.

surface may diffuse a distance on the Cu(100) surface, but is likely fairly soon to undergo place exchange with a surface Cu atom. The tendency of Fe atoms to cluster, due to the strength of Fe–Fe bonds, implies that other Fe atoms encountering the already embedded Fe atom will likely remain there. They may place-exchange with Cu atoms at neighboring sites, which forms a cluster embedded in the surface. This leads to the low-coverage structure shown in Figure 7(a). The Fe atoms may also encounter other Fe atoms and form a stable island *on* the surface, atop the embedded cluster. This creates a bilayer cluster, with buried atoms as measured by prior experiments. Such clusters are common as more Fe is deposited [Figure 7(b)]. Because part of the cluster is below the surface, like an iceberg, experiments sensitive to surface topography alone (such as diffraction oscillations and, usually, STM) will measure growth of *monolayer* islands. The Cu atoms released by place exchange also contribute to the aggregated first-layer islands.

This behavior is revealed in STM images in several ways. One indication is the heterogeneity of a one-monolayer deposit, which appears clearly when the sample is oxidized [31]. After one ML-equivalent of Fe has been deposited, the STM shows that about 80% of the first additional layer is filled, 20% of the second layer is filled (so that 80 − 20 = 60% of the first layer is *exposed*), and 20% of the surface is apparently uncovered. In the growth model, the first-layer aggregate consists of Cu as well as Fe. While this Fe–Cu heterogeneity does not typically show up as a pronounced contrast in the STM, it is made quite obvious by exposure of the sample to molecular oxygen. The Fe regions oxidize into a hexagonal FeO similar to that seen for oxidized Fe on Pt(111) [32], while the Cu regions remain unchanged [**Figure 7(c)**].

Another manifestation of the intermixing is easily measured with the STM but is somewhat subtle to interpret. This is the nucleation behavior of small islands and the size distribution of islands and clusters. The behavior of Fe on Cu(100) in this regard is inconsistent with the predictions of classical nucleation theory, whose successes were mentioned above, for free adatoms aggregating on an inert substrate. Under these conditions, the nucleation rate for new islands depends only on the number density of the diffusing gas of adatoms, which decreases as the number and size of islands (which absorb the adatoms) increases. Thus, the number of islands as a function of coverage, measured for each sample after all deposited atoms have attached to islands, should be concave downward; i.e., its derivative (the apparent nucleation rate) should be monotonically decreasing. For Fe on Cu(100) at room temperature, the nucleation rate for islands above the surface actually *increases* considerably at a coverage around 0.2 ML [**Figure 7(d)**]. This puzzling behavior arises because most islands form in a two-step

process: First, an embedded cluster is formed, and second, another layer of Fe grows atop the embedded Fe cluster, forming an "island." As a result, the number of islands grows faster than linearly, and thus has an increasing nucleation rate, until the absorption of adatoms ultimately pulls the nucleation back down. Other islands form by the usual combining of (Fe or Cu) adatoms on the surface. The two nucleation paths show up in the coexistence of a few fairly large islands with many much smaller ones. Under normal conditions the distribution should be less heterogeneous. We have also examined the size distribution of the embedded clusters, and compared it to different theoretical possibilities. The experimental results are consistent with the model that single Fe atoms can exchange with Cu in the substrate and, in so doing, become immobile [33].

A third indication is the direct observation of embedded Fe clusters. This is possible only at early stages (with less than 0.2 monolayer-equivalent of Fe deposited), when most of the embedded clusters are still exposed. The difference in chemistry and electronic structure between these clusters and the Cu surface causes a difference in apparent height that resembles the contrast seen for the patches discussed above for Fe on Au(111). The Fe–Cu contrast depends strongly on tip condition, which may change spontaneously or may be changed deliberately by application of a bias-voltage pulse of a few volts. An example of this dependence is shown in **Figure 8**. It is clear from this that the large and small features are different in structure and/or composition. It is not clear how the contrast occurs, but a strong apparent height difference may require an unusual arrangement of Fe, Cu, and/or other atoms on the tip that may form during a voltage pulse. Our identification of the different regions as embedded Fe clusters relies on their relationship, in a number of samples, to the amount of Fe deposited and to the temperature history of the sample [35]; it does not require that the origin of the Fe–Cu contrast be understood. Another group studying this system has not found the embedded Fe clusters [36], and it is not entirely clear whether the samples are truly different (perhaps because of somewhat different deposition temperatures) or whether the appropriate coverages and imaging conditions were not tried.

It should be noted that the exchange of Fe atoms with surface Cu does not violate thermodynamic driving forces, despite the Fe–Cu "immiscibility." This immiscibility can be regarded as a manifestation of a positive heat of mixing, or of Fe–Cu bonds that are somewhat weaker than the *average* of Fe–Fe and Cu–Cu bonds. Fe–Fe bonds are very much stronger than Cu–Cu bonds, as evidenced in their surface energy difference, and this difference is more important than the heat of mixing. Thus, Fe–Cu bonds are actually stronger than Cu–Cu bonds, and it is favorable to implant an Fe adatom into the surface. The configuration that minimizes free energy, which would be reached if the sample were allowed to equilibrate at elevated temperature, most likely involves 3D clusters of Fe completely surrounded by Cu so that there is no exposed Fe surface.

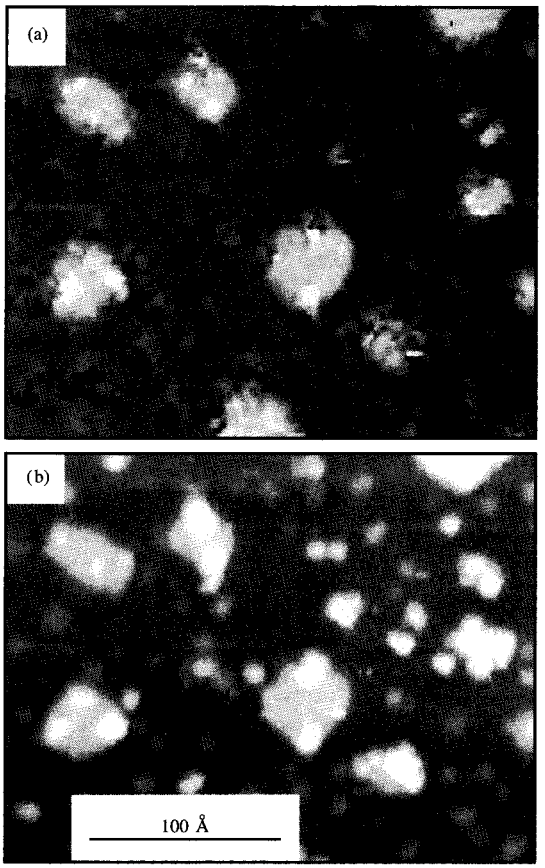

Figure 8

Evidence for subsurface Fe clusters on Cu(100). STM images of Cu(100) + 0.1 ML Fe show a mixture of larger and smaller features. Parts (a) and (b) show the same sample area imaged under the same applied conditions, (a) before and (b) after a spontaneous tip change. The large features (islands, mostly Cu) maintain the same appearance, but the appearance of small features (embedded Fe clusters) changes from pits to bumps when the tip changes [34].

Prior to microscopic studies of this sort, intermixing during epitaxy was regarded largely as a thermally excited process, so that it was surprising to find it to be important at room temperature. Thermal motion indisputably plays a part, but the driving force comes from the chemical reactivity of each atom that is deposited. A flux of single

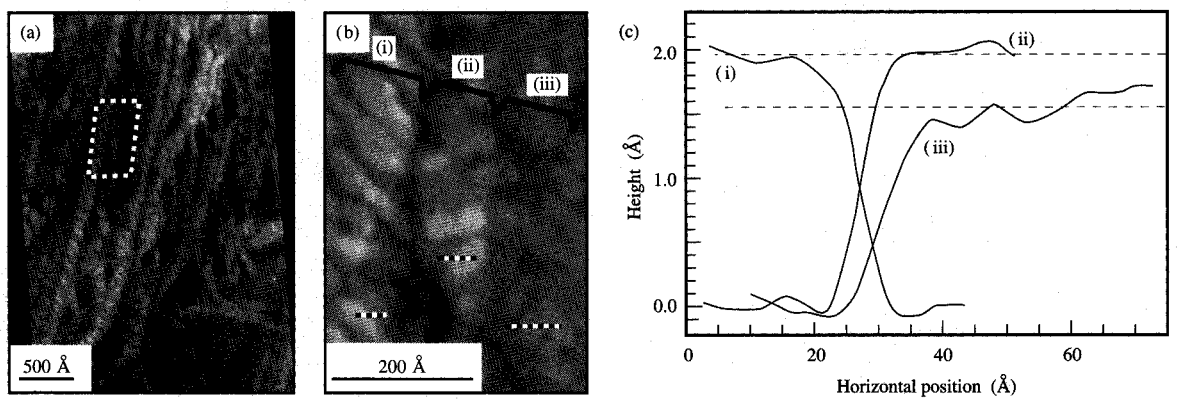

Figure 9

Bcc grain structure at 14 ML. (a) Long-range structure of sample after martensitic transformation. Marked outline indicates region shown in (b). (b) Step and island structure of fcc and bcc regions. (c) Step heights measured along dotted lines marked in (b) [41].

atoms contains a high density of chemical energy, much of which is not dissipated until the atoms have aggregated. It is not surprising that structures far from thermal equilibrium could be reached.

Higher-coverage Fe on Cu(100): Martensitic transformation

Thus far we have considered only submonolayer epitaxial deposits, which illustrate the principle that substrates cannot be regarded as inert. Epitaxial growth is a chemical reaction, and it should not seem strange that one of the reagents—the substrate surface—should sometimes have its structure disrupted. This principle extends to growth beyond the first monolayer in that each layer is the substrate for the next. While the exposed surface clearly presents opportunity for chemical reaction, one may still hope that layers already buried will not be significantly changed during further growth. It would be convenient if characterizing each monolayer with STM after its deposition were sufficient to know the final structure. Unfortunately, one cannot be sure this is the case. In this final section we discuss the later growth stages of Fe on Cu(100). In this system, the STM yields clear evidence that significant structural change goes on below the surface [37]. The change is an example of a martensitic transformation,[1] described below. Martensitic transformations are well known in bulk metallurgy, and are essential to the heat treatment of steels, but they had not previously been recognized as important for thin films on crystal substrates.

Fe grows at coverages below about 14 ML nearly layer-by-layer on Cu(100), in an fcc-like structure which is apparently pseudomorphic to the substrate [33, 38]. The initial layers are disrupted somewhat by the intermixing discussed above, but once the Cu surface is buried, there is a repeated cycle of island nucleation, island growth, and layer completion typical of layer growth. STM images show that only two or three exposed layers account for almost the entire surface. The Fe film is not in its bulk-stable body-centered cubic (bcc) structure, however, and before coverage of 20 ML is reached, there is a transition into a polycrystalline bcc film. The bcc grains generally have one close-packed direction nearly parallel to a close-packed row of the substrate, and the close-packed (110) surface parallel to the substrate surface [39]. Low-energy electron diffraction (LEED) and STM have confirmed a transition to a bcc(110) surface, thus oriented, at thicknesses between 10 ML and 14 ML [40].

STM images of a 14-ML deposit (**Figure 9**) are markedly different from typical images of metal crystals with flat terraces and clear steps (cf. Figures 2 and 5). This is a complicated surface with different regions. The most apparent features in a wide-range view [Figure 9(a)] are linear ridges running predominantly along the two close-packed directions of the original surface. These ridges prove to be narrow, long (typically 200-Å × 3000-Å) bcc grains. There also remain some regions that resemble the surface of the fcc-like film. These are parts of the film that have not yet been converted to bcc. A closer view [Figure 9(b)] shows the differences between bcc- and fcc-like parts

[1] An interesting introduction is offered by J. Sethna et al. as a WorldWide Web page with URL:
http://www.lassp.cornell.edu/sethna/Tweed/What_Are_Martensites.html.

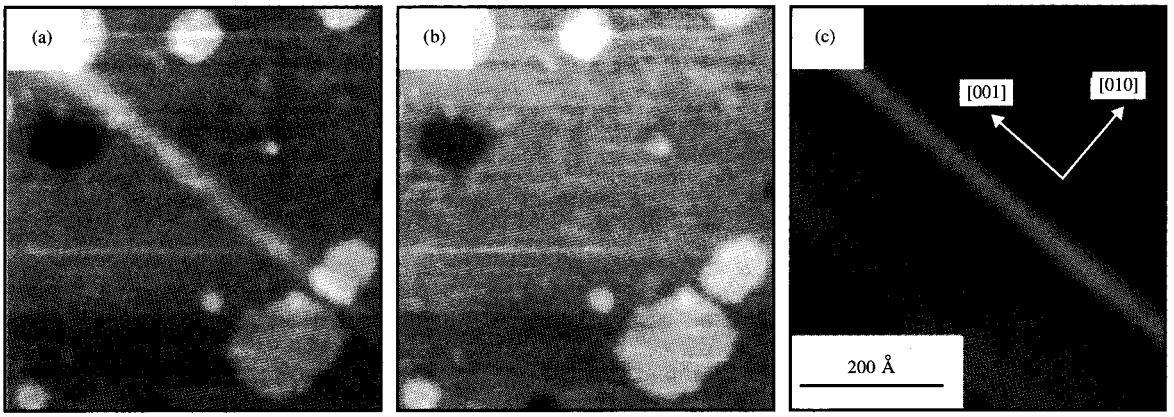

Figure 10

Subsurface structural change: (a) STM image of 10 ML Fe grown on Cu(100). Light diagonal band is ridge caused by subsurface structural change. (b) Data of (a) with ridge subtracted numerically. (c) Topography of ridge, estimated by averaging heights in (a) along [001] direction parallel to ridge.

of the sample. The two bcc regions (i and ii) exhibit a significantly higher step height than the fcc region (iii) [Figure 9(c)], which is consistent with the difference in interplanar spacing between fcc–Fe(100) and bcc–Fe(110). Concurrent with the change in step height is a significant increase in average height of the surface of the transformed region.

The island growth characteristics in bcc and fcc regions are different. Growth on a bcc grain yields islands elongated along the bcc [001] direction, at an angle of 55° to the close-packed $[1\bar{1}1]$ axis of the grain. Some of this can be seen in region (i), whereas in (ii) there is little island growth with this character. The explanation is that only growth subsequent to the local transformation exhibits this characteristic, and region (ii) was converted to a bcc structure shortly before deposition was complete. By examining many regions of the sample, we know that the structural change does not significantly rearrange atoms on the surface, but instead applies a uniform geometric transformation to the transformed region as a whole. Thus, islands are preserved, although their shapes are distorted. Surface steps are often found that cross an fcc–bcc boundary with no apparent disruption except a shift in height and possibly along the direction of the boundary. They resemble in this respect the fences and roads that cross earthquake fault lines that are particularly active.

An example of subsurface change is seen in **Figure 10**. The ridge seen in the STM data (a) is due to a subsurface structural change. The STM heights are expressed as the sum of image (b), which presumably approximates the surface topography before the change, with (c), which is the ridge cross section across [010], averaged along [001]. The significant observation is that the surface texture in (b) shows no indication of where the ridge is. Thus the formation of the ridge here has not significantly changed the surface atomic structure.[2]

The behavior of the surface as Fe is deposited is a clear indication that a structural change goes many layers deep, and is a collective motion of all the atoms in the region instead of an aggregate of independent random motions. This is the main characteristic of a martensitic transformation. Martensitic transformations are common in bulk ferrous alloys and, as is the case here, are typically identified by the grain shapes and orientations that result. Such a transformation is essentially a shear along a close-packed direction [**Figure 11(a)**] combined with small expansions, contractions, and rotations because of the change in nearest-neighbor spacing. For the fcc–bcc transition here, it results in approximately the crystallographic relationship illustrated in Figure 11(a) [42]. The transformation of part of a thin film may be envisioned as in **Figure 11(b)**. One boundary with the fcc parent phase is the invariant plane A, with no slip. There must be slip between the parent and the martensite at B, unless it is eliminated by a slip or twin boundary within the martensite grain. The collective motion forming a martensite grain leads to a highly anisotropic shape and to particular angles

[2] For most martensite grains, the surface texture is correlated to the ridge topography: The fcc → bcc change tends to make the surface smoother and skew the island edges. Thus, the ridge shown here might not be a martensitic grain, but rather a dislocation that does not disturb the surface atomic structure.

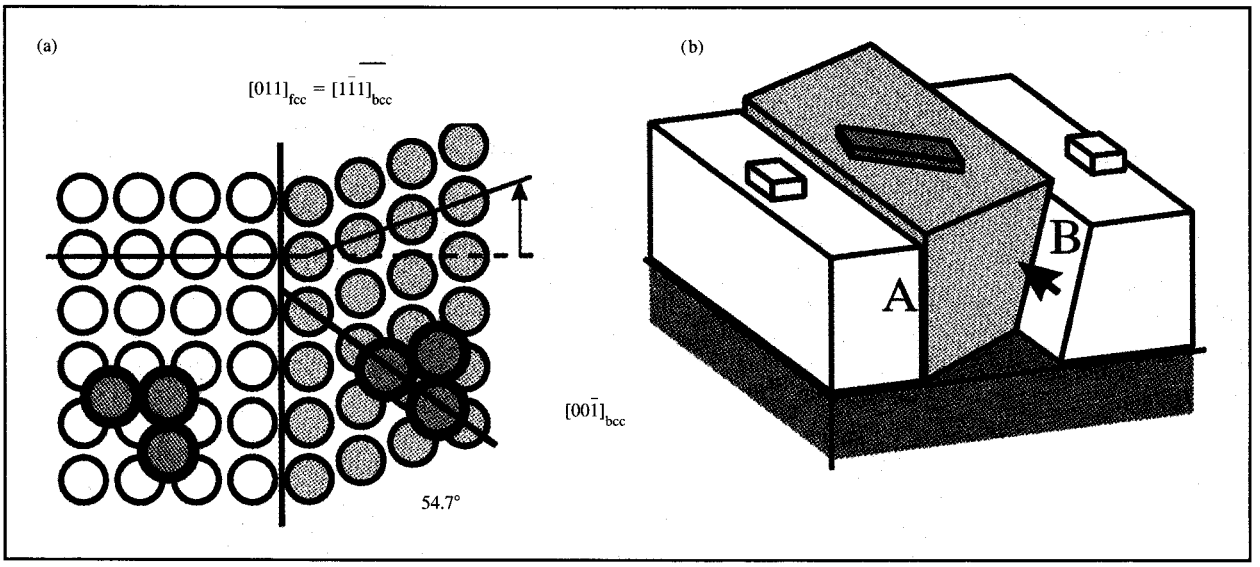

Figure 11

Martensitic transformation: (a) Orientational relationship between a bcc–Fe(110) surface and pseudomorphic fcc–Fe(100) on Cu(100) (plan view). The fcc–bcc change is mainly a shear (arrow) along a shared close-packed direction. Adatoms (heavy circles) are in fourfold-hollow sites on fcc(100), long bridge sites on bcc(110); favored steps on bcc(110) lie along $[001]_{bcc}$. (b) Thin-film martensitic grain. Martensite (shaded) forms by shear (arrow) plus expansions/contractions [37].

between the grain and its parent phase. Any growth on the surface of the martensite will respond to the changed symmetry and chemistry implied by the structural transformation.

These observations are instructive both for the usefulness of STM and for our understanding of epitaxial growth. Although the STM only observes the surface, it has nevertheless been possible to identify a transformation in the bulk of a film by its surface manifestations. The angles of growth and step heights allow one to infer that bcc–Fe(110) grains are present. One still needs a probe such as diffraction to establish this with certainty. The significant change in average height, and the behavior of steps, show that many layers in the film must be involved in the transformation. Perhaps most important, the coexistence side by side of bcc and fcc Fe in this sample, and for a range of other Fe thicknesses, would not have been clearly known without a microscopic probe.

The dramatic change in surface appearance that occurs in the fcc–bcc transition underscores the structural instability of the pseudomorphic Fe film, and the possibility for more subtle distortions even before the transformation. There are many indications that the fcc-like Fe on Cu(100) is not energetically stable. The fcc–Fe films show a variety of reconstructions depending on coverage and film preparation [38, 43, 44], and these appear to involve shear displacements similar to those involved in the fcc–bcc transformation. Recent medium-energy ion-scattering results [45] indicate that the Fe is distorted in complex ways, apparently being non-pseudomorphic and rotated with respect to the Cu lattice. This is consistent with our STM observation that the "atomically flat" surfaces of the fcc-like Fe in fact show significant roughness (0.1 Å rms) [37]. Most of this roughness goes away when the fcc–bcc transformation takes place. It appears that there is a strong tendency toward local bcc-like bonding, which produces local distortions until the activation barrier to form long-range bcc order can be overcome.

A more general conclusion is that metastable epitaxial structures must be regarded with some caution. As layers are buried, they may be protected from the chemical reaction of direct intermixing, but they are still subject to bulk-like transformations. The latent energy of the structural change remains available in the film, so a small stimulus (perhaps at the surface) might be enough to trigger a change that propagates into the bulk of the film. In the fcc–bcc samples discussed above, typically 10^5–10^6 atoms were involved in the transformation of each grain. An additional caution is that the possibility of structural heterogeneity across the surface must be kept in mind. At an early stage of the fcc–bcc transition, for example, bcc grains covering 10% of the surface could yield contributions to magnetic properties that could easily be misattributed to the fcc-like iron.

Conclusion

The STM's capability of revealing microscopic surface structure at an atomic level has advanced considerably our understanding of epitaxial growth. It has allowed us and other groups to confirm and refine many of the atomistic concepts for nucleation and growth that were formulated long before they could be observed in such detail. This capability has also led to surprises that challenge the assumptions behind those established theories. The dynamic character of the substrate, and in particular the possibility of atomic place exchange, play a more significant role in epitaxy than has been appreciated in the past. A wider range of defect structures in surfaces and films has been found than had been anticipated, which leads both to new concerns and to new possibilities. The surprising results that have arisen from STM studies of epitaxy indicate that further studies will be a rich source of new information.

Acknowledgments

These studies would not have been possible without the hard work and scientific insight of Kevin Johnson, Kathrin Kalki, Phil Lippel, Sylvie Rousset, Bruce Melior, David Fowler, and Christof Wöll. This work has been funded in part by the Office of Naval Research (N00014-89-C-0099).

References

1. A. K. Schmidt and J. Kirschner, *J. Vac. Sci. Technol. B* **9,** 649 (1991).
2. J. A. Stroscio, D. T. Pierce, and R. A. Dragoset, *Phys. Rev. Lett.* **70,** 3615 (1993).
3. J. Sudijono, M. D. Johnson, C. W. Snyder, M. B. Elowitz, and B. G. Orr, *Phys. Rev. Lett.* **69,** 2811 (1992).
4. D. D. Chambliss and K. E. Johnson, *Surf. Sci.* **313,** 215 (1994).
5. J. A. Venables, G. D. T. Spiller, and M. Hanbücken, *Rep. Progr. Phys.* **47,** 399 (1984).
6. S. Chiang, R. J. Wilson, C. Gerber, and V. M. Hallmark, *J. Vac. Sci. Technol. A* **6,** 386 (1988).
7. W. E. Egelhoff, *J. Vac. Sci. Technol. A* **3,** 1511 (1985).
8. U. Harten, A. Lahee, J. Toennies, and C. Wöll, *Phys. Rev. Lett.* **54,** 2619 (1985).
9. C. Wöll, S. Chiang, R. J. Wilson, and P. H. Lippel, *Phys. Rev. B* **39,** 7988 (1989).
10. D. D. Chambliss and R. J. Wilson, *J. Vac. Sci. Technol. B* **9,** 928 (1991).
11. J. V. Barth, H. Brune, G. Ertl, and R. J. Behm, *Phys. Rev. B* **42,** 9307 (1990).
12. S. Narasimhan and D. Vanderbilt, *Phys. Rev. Lett.* **69,** 1564 (1992).
13. M. Bott, M. Hohage, T. Michely, and G. Comsa, *Phys. Rev. Lett.* **70,** 1489 (1993).
14. J. V. Barth, Ph.D. thesis, Freien Universität Berlin, Germany, 1992.
15. K. G. Huang, D. Gibbs, B. M. Ocko, D. M. Zehner, A. R. Sandy, and S. G. J. Mochrie, *Phys. Rev. Lett.* **65,** 3313 (1990).
16. D. D. Chambliss, R. J. Wilson, and S. Chiang, in *Structure/Property Relationships for Metal/Metal Interfaces*, A. D. Romig, D. Fowler, and P. D. Bristowe, Eds., Materials Research Society, Pittsburgh, 1991, p. 15.
17. D. D. Chambliss and R. J. Wilson, *J. Vac. Sci. Technol. B* **9,** 928 (1991).
18. T. A. Whitten and L. M. Sander, *Phys. Rev. Lett.* **47,** 1400 (1981).
19. L. Kadanoff, *J. Stat. Phys.* **39,** 267 (1985).
20. R. Q. Hwang, J. Schröder, C. Günther, and R. J. Behm, *Phys. Rev. Lett.* **67,** 3279 (1991).
21. D. D. Chambliss, R. J. Wilson, and S. Chiang, *Phys. Rev. Lett.* **66,** 1721 (1991).
22. P. J. Feibelman, *Phys. Rev. Lett.* **65,** 729 (1990).
23. G. L. Kellogg and P. J. Feibelman, *Phys. Rev. Lett.* **64,** 3143 (1990).
24. S. Rousset, S. Chiang, D. E. Fowler, and D. D. Chambliss, *Phys. Rev. Lett.* **69,** 3200 (1992).
25. P. Fenter and T. Gustafsson, *Phys. Rev. Lett.* **64,** 1142 (1990).
26. C. T. Chan, K.-P. Bohnen, and K. M. Ho, *Phys. Rev. Lett.* **69,** 1672 (1992).
27. M. I. Haftel, M. Rosen, T. Franklin, and M. Hettermann, *Phys. Rev. Lett.* **72,** 1858 (1994).
28. D. D. Chambliss and S. Chiang, *Surf. Sci. Lett.* **26,** L187 (1992).
29. D. A. Steigerwald and J. W. F. Egelhoff, *Phys. Rev. Lett.* **60,** 2558 (1988).
30. S. A. Chambers, T. J. Wagener, and J. H. Weaver, *Phys. Rev. B* **36,** 8992 (1987).
31. K. E. Johnson, D. D. Chambliss, R. J. Wilson, and S. Chiang, *J. Vac. Sci. Technol. A* **11,** 1654 (1993).
32. H. C. Galloway, J. J. Benítez, and M. Salmeron, *Surf. Sci.* **298,** 127 (1993).
33. D. D. Chambliss and K. E. Johnson, *Phys. Rev. B* **50,** 5012 (1994).
34. D. D. Chambliss, *J. Vac. Sci. Technol. A* **10,** 1993 (1992).
35. K. E. Johnson, D. D. Chambliss, R. J. Wilson, and S. Chiang, *Surf. Sci. Lett.* **313,** L811 (1994).
36. J. Shen, J. Giergiel, A. K. Schmid, and J. Kirschner, *Surf. Sci.* **328,** 32 (1995).
37. K. Kalki, D. D. Chambliss, K. E. Johnson, R. J. Wilson, and S. Chiang, *Phys. Rev. B* **48,** 18344 (1993).
38. J. Thomassen, B. Feldmann, and M. Wuttig, *Surf. Sci.* **264,** 406 (1992).
39. J. Koike and M. Nastasi, in *Evolution of Thin Film and Surface Microstructure*, C. Thompson, J. Tsao, and D. Srilovitz, Eds., *Proceedings of the Materials Research Society*, Vol. 202, p. 13.
40. M. Wuttig, B. Feldmann, J. Thomassen, F. May, H. Zillgen, A. Brodde, H. Hannemann, and H. Neddermeyer, *Surf. Sci.* **291,** 14 (1993).
41. D. D. Chambliss, K. E. Johnson, K. Kalki, R. J. Wilson, and S. Chiang, in *Magnetic Ultrathin Films: Multilayers and Surfaces, Interfaces and Characterization*, B. T. Jonker et al., Eds., *Proceedings of the Materials Research Society*, 1993, pp. 713–722.
42. C. M. Wayman, in *Physical Metallurgy*, R. W. Cahn and P. Haasen, Eds., North-Holland Publishing Co., New York, 1983, pp. 1031–1074.
43. W. Daum, C. Stuhlman, and H. Ibach, *Phys. Rev. Lett.* **60,** 2741 (1988).
44. D. P. Pappas, K.-P. Kämper, and H. Hopster, *Phys. Rev. Lett.* **64,** 3179 (1990).
45. J. Barth and D. Fowler, *Phys. Rev. B.* **152,** 1528 (1995).

Received November 22, 1994; accepted for publication July 31, 1995

David D. Chambliss *IBM Research Division, Almaden Research Center, 650 Harry Road, San Jose, California 95120 (CHAMB at ALMADEN, chamb@almaden.ibm.com).*
Dr. Chambliss has been a research staff member at the IBM Almaden Research Center since 1991 in the Magnetic Materials and Phenomena Department. He received a Ph.D. degree in applied physics from Cornell University in 1989, and did postdoctoral research at the IBM Almaden Research Center from 1989 to 1991. His research interests are surface science and materials physics, with an emphasis on epitaxial growth and the magnetic properties of thin metal films, studied using scanning tunneling microscopy and spin-polarized low-energy electron microscopy. Dr. Chambliss is a member of the American Physical Society and the American Vacuum Society.

Robert J. Wilson *IBM Research Division, Almaden Research Center, 650 Harry Road, San Jose, California 95120 (WILSON at ALMADEN, wilson@almaden.ibm.com).*
Dr. Wilson has been a research staff member at the IBM Almaden Research Center since 1983 in the Science and Technology Department. He received a Ph.D. degree in physics from the University of California at Berkeley and has done postdoctoral research at Bell Laboratories. His research interests in condensed matter physics and surface science include the structure of metal films grown by evaporation and sputter deposition, and the behavior of organic molecules on surfaces.

Shirley Chiang *Department of Physics, University of California at Davis, Davis, California 95616 chiang@physics.ucdavis.edu).* Dr. Chiang has been a professor of physics at the University of California at Davis since 1994. She received her Ph.D. degree in physics from the University of California at Berkeley in 1983 and was a research staff member at the IBM Almaden Research Center in San Jose from 1983 to 1994. Her research interests are in condensed matter physics and surface science. She specializes in scanning tunneling microscopy in an ultrahigh-vacuum environment for studies of epitaxial growth of metals on metals and high-resolution imaging of small molecules on metals. Dr. Chiang is a member of the American Physical Society, the American Vacuum Society, and the Materials Research Society.